IEEE Access
Multidisciplinary | Rapid Review | Open Access Journal

Received April 6, 2021, accepted April 23, 2021, date of publication April 29, 2021, date of current version May 12, 2021.

Digital Object Identifier 10.1109/ACCESS.2021.3076631

Fading Evaluation in Standardized 5G Millimeter-Wave Band

TIAGO REIS RUFINO MARINS[1], ANDRÉ ANTÔNIO DOS ANJOS[1], CARLOS RAFAEL NOGUEIRA DA SILVA[2], VICENT MIQUEL RODRIGO PEÑARROCHA[3], LORENZO RUBIO[3], (Senior Member, IEEE), JUAN REIG[3], (Senior Member, IEEE), RAUSLEY ADRIANO AMARAL DE SOUZA[1], (Senior Member, IEEE), AND MICHEL DAOUD YACOUB[4], (Member, IEEE)

[1]National Institute of Telecommunications-INATEL, Santa Rita do Sapucaí 37540-000, Brazil
[2]Department of Electrical Engineering, Federal University of Triângulo Mineiro (UFTM), Uberaba 38025-180, Brazil
[3]Telecommunications and Multimedia Applications Research Institute (iTEAM), Universitat Politècnica de València, 46022 Valencia, Spain
[4]Wireless Technology Laboratory (WissTek), Department of Communications(DECOM), School of Electrical and Computation Engineering, State University of Campinas (UNICAMP), Campinas 13083-852, Brazil

Corresponding author: Rausley Adriano Amaral De Souza (rausley@inatel.br)

This work was supported in part by the Rede Nacional de Ensino e Pesquisa (RNP) with resources from Ministério da Ciência, Tecnologia e Inovações (MCTIC) through the 6G Mobile Communications Systems Project of the Centro de Referência em Radiocomunicações (CRR), Instituto Nacional de Telecomunicações (Inatel), Brazil, under Grant 01245.010604/2020-14, in part by the Fundação de Amparo à Pesquisa do Estado de Minas Gerais (FAPEMIG), in part by the Conselho Nacional de Desenvolvimento Científico e Tecnológico (CNPq) under Grant 304248/2014-2, and in part by the Ministerio de Economía, Industria y Competitividad of the Spanish Government under the National Project through the Agencia Estatal de Investigación (AEI) and the Fondo Europeo de Desarrollo Regional (FEDER) under Grant TEC2017-86779-C2-2-R.

ABSTRACT Recent standardization of portions of the millimeter-wave (mm-wave) band for fifth-generation (5G) operation has called for further research on how short-term fading behaves in that unexplored part of the spectrum. With such a target, this paper reports on a thorough measurement campaign conducted in an indoor environment characterized by rich-multipath scattering, a part of a modern building, with floor and ceiling constructed of reinforced concrete over steel plates with wood and plasterboard-paneled walls. Particularly, measurements have been performed in a variety of scenarios, under line-of-sight (LoS) and non-line-of-sight (nLoS) conditions, for a wide range of frequencies, namely from 25 to 40 GHz - a span of 15 GHz - therefore, including 26, 28 and 39 GHz. First and second order statistics of representative fading models, namely Rayleigh, Rice, Nakagami, folded normal, α-μ, η-μ, κ-μ, and α-η-κ-μ have been investigated. The metrics used in the analysis were the normalized mean square error (NMSE), the Kolmogorov-Smirnov (KS), and the Akaike information criterion (AIC). Additionally, the study of the κ-μ model is advanced, in which new, exact, simple closed-form expressions for probability density function, cumulative distribution function, and level crossing rate are derived for some particular cases, namely for $\mu = n + 1/2$ in which $n \in \mathbb{N}$.

INDEX TERMS Fading model, wireless channel, 5G-NR, multipath fading, mm-wave.

I. INTRODUCTION

The primary requirement for the emergence of any advanced generation wireless communications system (e.g. 5G and beyond) is the provision for larger bandwidth so that, what is claimed to be its flagship, i.e. the convergence of a variety of services, can be fully implemented. Larger bandwidth is a rather scarce resource at lower frequency band. Hence the obvious, though bold, step is to move toward higher frequency bands - mm-wave band ((20)30 GHz to 300 GHz) -, where the availability of and, unfortunately, the lack of familiarity with the spectrum are certain.

Recently, in the last World Radio Communications Conference (WRC) of the International Telecommunication Union (ITU), held in 2019, the 26, 28 and 39 GHz frequency bands were approved to comply with the fifth-generation new radio (5G-NR) high throughput scenarios [1]. These bands, as the mm-wave band in general, facilitate the deployment of pico- or even nano-cell structures but offer great challenges. Maximum radio communication range is one of them when compared with that of systems operating in the ultra-high frequency (UHF) band (30 MHz to 300 MHz). Other challenges include how the atmospheric conditions affect the

The associate editor coordinating the review of this manuscript and approving it for publication was Vittorio Degli-Esposti.

propagation scenario for both direct path (LoS), with dominant components, or indirect paths (nLoS), with reflections and diffraction through the various surfaces.

A significant number of measurement campaigns at the mm-wave band has been conducted with the aim at characterizing the propagation channel [2]–[15]. As a matter of fact, most of those works explore the large-scale propagation phenomenon. For instance, in [2], the authors use measurements at 28 and 73 GHz conducted in New York city to derive metrics such as path loss, number of spatial clusters, angular dispersion, and outage probability. In [3], the path loss characteristics of indoor environments based on measurements are derived using omnidirectional and horn antennas for both LoS and nLoS scenarios at 60 GHz. In [4], the authors use a spectrum analyzer and a synthesized signal generator to perform several measurements for the frequency-domain characterization of the radio channel in the 60 GHz band. In the experiments, a carrier wave with a constant amplitude sweeps across the 100 MHz band, centered around 59.9 GHz. In [5], the channel characteristics of mm-wave at 39 GHz in indoor environments based on channel measurements in a conference room and in a lobby are analyzed. Path loss, shadowing, and small-scale fading statistics encompassing the Rice factor, root mean square (RMS) delay spread, and RMS angular spread are presented. Some results for wireless channels at 15 and 28 GHz in an indoor scenario are presented in [5]. The results are based on both measurements and ray-tracing simulations. Basic comparisons of measured and simulated power-delay profiles, angle of departure, and received power are presented. Interestingly, human body shadowing, as well as finer structures, are taken into consideration.

The statistics of small-scale fading at mm-wave frequencies have thus far received little attention. In addition, in most of the few studies available in the literature covering measurements in mm-wave to characterize short-term fading in nLoS and LoS scenarios, most frequently Rayleigh and Rice statistics are considered [10], [11], [16]–[18]. In [16], the short-term fading amplitude for LoS measurements taken in three corridors of an office block at frequency 60 GHz with a bandwidth of 1 GHz is modeled with a Rician distribution. Values of the mean and standard deviation of the Rice factor are reported for two antenna types, i.e. an open-ended waveguide and lens. Other interesting results are shown in [17], where the small-scale fading statistics obtained from a 28 GHz outdoor measurement campaign reveals that the Rician model is more suitable than Rayleigh even in nLoS conditions. Some other related investigations concerning short-term fading in mm-wave [17]–[19] concludes that more generalized fading models need to be evaluated so that the behavior of the fading channel can be better captured.

The newness of the propagation scenario at the mm-wave band calls for a thorough investigation particularly as far as the short-term statistics are concerned. More conventional fading models, e.g. Rayleigh, Hoyt, Rice, Nakagami, and Weibull, as well as less conventional ones, e.g. α-μ, κ-μ, and η-μ, may serve this purpose. In addition to these, three other less known models are of interest. The first one is the folded normal (FN), a direct particularization of the κ-μ with $\mu = 1/2$, here also named κ-$1/2$, which has a very elementary functional form and which has been successfully used in [20]. The second one is another particularization of κ-μ, with $\mu = 3/2$, also presented in simple functional form, and here named κ-$3/2$. The third one is the α-η-κ-μ, which is a very general fading model, and which is able to accommodate an enormous number of fading scenarios, due to its multi-parameter characteristic. And exactly because of this, it is indeed more mathematically involving. All the aforementioned cases shall be explored here.

In this paper a mm-wave measurement campaign is carried out in a lab environment aiming at characterizing the first and the second-order short-term fading channel behavior in the frequencies 26, 28, and 39 GHz, standardized by the ITU for the new generations of mobile communications 5G-NR. To the best of the authors' knowledge, such a thorough characterization in this newly allotted 5G band, even more, considering also generalized fading models is unprecedented in the literature. A wide range of measurements is conducted in a variety of scenarios. Different fading models are tested, namely Rayleigh, Rice, Nakagami, α-μ, κ-μ, FN, η-μ, and α-η-κ-μ. From the experimental data, the parameters of these models are estimated and the corresponding curves of the theoretical models are compared with the empirical ones and the best model is selected. In addition, motivated by the fact that a particular case of the κ-μ model, namely FN, has its probability density function (PDF) given in a very simple functional form, other particular cases of κ-μ model, namely those for $\mu = n + 1/2$ in which $n \in \mathbb{N}$, are obtained in terms of elementary functions (PDF and level crossing rate (LCR)) or in terms of computationally more efficient forms (cumulative distribution function (CDF)). Here again, to the best of the authors' knowledge, the derivations given are unprecedented in the literature.

This paper is organized as follows. Section II briefly refers to the PDFs and LCRs expressions used for the fading models under test and revisits the goodness-of-fit (GoF) methods used. Section III provides closed-form expressions for first- and second order statistics, given in terms of elementary functions, for useful particular cases of the κ-μ model. The measurement setup and the measurement environment are described in Section IV. Section V analyzes the numerical results obtained from the measured data. Finally, Section VI draws some conclusions.

II. PRELIMINARIES

A. FADING MODELS

As already mentioned, the fading models under test are Rayleigh, Rice, Nakagami, α-μ, κ-μ, FN, η-μ, and α-η-κ-μ. The expressions of their first-order statistics, namely PDF, as well as the description of the corresponding parameters can be found in [21]. In the same way, the expressions of their second-order statistics, namely LCR, as well as the

description of the corresponding parameters can be found in [22]. In both cases, the formulations for the FN can be easily obtained in a straightforward form from those of κ-μ ones by setting $\mu = 1/2$.

B. GoF TESTS

In the analyses conducted here, three different figures of merit or criteria are used to verify which theoretical model best fits the empirical data [23]. The NMSE is used for analyses in which the focus is to compare the empirical curve (PDF or LCR) and the theoretical one in order to quantify the curves dissimilarity (mean distance). Its units are given in dB to highlight the differences at the lower part of the distribution. The KS test is performed so that the estimated CDF and the hypothesized CDF are compared. Finally, the AIC is used to compare empirical and theoretical statistical distribution models considering dissimilarity, quantity of samples, and number of parameters of the distribution. In NMSE and AIC tests, the chosen distribution is the one with the lowest value. The KS statistical parameter D represents the maximum absolute difference between theoretical and empirical distributions. If the sample comes from a given distribution, then D converges to zero almost surely in the limit as the sample size tends to infinity. The corresponding p-value is calculated based on the KS parameter D and it represents the reliability of the test considering a given confidence interval. The best-fitting performance is achieved by the distribution presenting the lowest D value and highest p-value. Note that these are statistical models using different criteria. As such, there is no one single criterion that is universally accepted to yield the indisputable result. Hence, owing to the fact that any statistical test uses different approach, the conclusions drawn from the one will not necessarily coincide with those from the other. And this is quite understood.

III. EXACT, SIMPLER CLOSED-FORM EXPRESSIONS FOR κ-μ FADING MODEL

The PDF of the κ-μ fading model, for the full range of its parameters, is invariably written in terms of special functions such as the modified Bessel function or the hypergeometric function, and sometimes it is even given as an infinite summation. In [20], a particular case of the κ-μ model, namely FN, obtained from it by setting $\mu = 1/2$, was used to fit field data. The advantage of FN is that its PDF is given in terms of elementary function rendering it mathematically easily manageable. Motivated by this, other particular cases of the κ-μ model with simpler functional forms are pursued. Particularly, it is found that for $\mu = n + 1/2$ in which $n \in \mathbb{N}$, both the PDF and the LCR can be put in terms of elementary functions and the CDF is found in efficiently computational form.

We intend here to provide an alternate formulation for the κ-μ PDF given only in terms of elementary functions.

Let $\mu = n + 1/2$ in which $n \in \mathbb{N}$. Then the normalized PDF of the κ-μ fading model can be written as (1), as shown at the bottom of the next page, where $\lfloor x \rfloor$ denotes the floor function, ρ the normalized short-term signal amplitude, and κ and μ are the parameters of the distribution. Note that this expression is in the closed-form and is given only in terms of powers and exponential of the variable ρ. This expression is obtained by using [24, Eq. (03.02.03.0006.01)] to write the Bessel function in terms of a finite summation of powers modulated by hyperbolic sine and cosine. Proceeding with algebraic manipulations the desired expression is found.

The PDF given by (1) allows for the derivation of a closed-form expression for the κ-μ CDF in terms of the incomplete gamma function, which computes more efficiently than the Marcum-Q function. Through the CDF definition, after some algebraic manipulation two similar integrals, L_1 and L_2, arise as

$$L_n = \int_0^{\rho} z^{\mu-\frac{1}{2}-i-2J} e^{-\mu(1+\kappa)\left(z-(-1)^n\sqrt{\frac{\kappa}{1+\kappa}}\right)^2} dz. \qquad (2)$$

They can be solved with the help of [25, Eq. (1.3.3.18)]. After tedious algebraic manipulations the CDF is found as in (3), as shown at the bottom of the page 5, where $\Gamma(a, b)$ is the lower incomplete gamma function [26, Eq. (6.5.2)] and $\text{sign}(x) = |x|/x$ is the signum function.

In the same way as the PDF and CDF, the LCR can also be obtained in terms of elementary functions. Let $\mu = n + 1/2$ with $n \in \mathbb{N}$, then the LCR of the κ-μ is obtained as (4), as shown at the bottom of the page 5. A consequence is that the κ-μ average fade duration (AFD) can also be obtained in terms of simpler function. The AFD is defined as $T_R(\rho) = F_R(\rho)/N_R(\rho)$, both here given in terms of elementary functions or the gamma functions. To the best of the authors' knowledge the expressions derived here are new.

The formulations specialized for κ-3/2 and κ-1/2 (FN) are shown in equations (5) and (6), as shown at the bottom of the page 5, for the PDFs, (7) and (8), as shown at the bottom of the page 5, for the CDFs, and (9) and (10), as shown at the bottom of the page 5, for the LCRs, respectively, where $Q(x) = 1/\left(\sqrt{2\pi}\right) \int_x^{\infty} \exp\left(-u^2/2\right) du$ and $\cosh(\cdot)$ is the hyperbolic cosine.

IV. CHANNEL MEASUREMENTS

A. PROPAGATION ENVIRONMENT

The channel measurements were carried out in a laboratory of the iTEAM Research Institute at the Universitat Politècnica de València, Spain. The dimensions of the laboratory are 13.5-m-long, 7-m-width and 2.6-m-high. This environment is characterized by rich-multipath, with scattered and reflected contributions, due to the presence of radio-frequency equipment, metallic cupboards, multiple work tables, desks, and benches equipped with electronic devices and chairs, among others. This laboratory is part of a modern building construction, where floor and ceiling are constructed of reinforced concrete over steel plates with wood and plasterboard-paneled walls. Fig. 1 shows a view of the propagation environment.

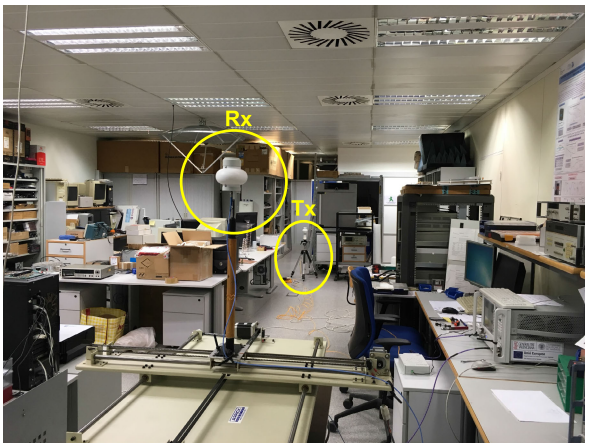

FIGURE 1. View of the propagation environment with the Tx (position 1) and Rx antennas.

B. MEASUREMENT SETUP

The channel transfer function (CTF) was measured in the frequency domain using a channel sounder based on the Keysight PNA N5227 vector network analyzer (VNA). This channel sounder was used in other scenarios [27], [28] to perform channel measurements at mm-wave frequencies. The Q-PAR QOM-SL-0.8-40-K-SG-L ultra-wideband antennas, with vertical polarization and omnidirectional radiation pattern in azimuth (horizontal plane), were used at the transmitter (Tx) and receiver (Rx) sides. The 3 dB beamwidth of the antennas in the elevation plane ranges from 20° to 40 ° in the 25-40 GHz frequency band, and the 10 dB beamwidth ranges from 45° to 100°.

The Tx subsystem was connected to the VNA through a radio over fiber (RoF) link to avoid the high attenuation of coaxial cables at mm-wave frequencies, thus expanding both the dynamic range in the measurements and the Tx-Rx distance. A schematic of the channel sounder is shown in Fig. 2. The Rx antenna was located on a XY linear positioning system emulating a $N \times M$ uniform rectangular array (URA) with an interelement separation of 1.01 mm, which corresponds to a separation close to $\lambda/8$ at 40 GHz. A personal computer controlled both the VNA and the XY positioning system, measuring the $S_{21}(f)$ scattering parameter which is equivalent to the CTF. The span used is of 15 GHz, from 25 to 40 GHz, in 16 frequency bins with a separation between consecutive frequency bins of 1 GHz. The advantage of this measurement method is to analyze and compare the behavior of the propagation channel at the 26, 28 and 39 GHz bands in the same propagation conditions. A response calibration of the channel sounder was performed prior to the measurements. The bandwidth of the intermediate frequency (IF) filter at the VNA was set to 100 Hz. This value guarantees an adequate trade-off between acquisition time and measuring dynamic range in the frequency bands considered.

TABLE 1. Characteristics of the positions.

Positions	Tx-Rx separation (m)	Condition	Scenarios
1	7.73	LoS	1
2	7.78	LoS and nLoS	2 and 3
3	5.61	LoS	4
4	4.36	LoS	5
5	4.91	LoS	6

The Tx antenna was mounted on a tripod, with a height of 0.90 m, imitating a user equipment (UE). The Rx subsystem remained fixed in the same location, imitating the position of an access point (AP), the Rx antenna height was 1.65 m. Five positions for the Tx antenna were considered with LoS propagation conditions. The dimensions of the URA were 90×750, that corresponds to a small-local area of about $12\lambda \times 100\lambda$. In position 2, two measurements were carried out, in LoS and nLoS conditions. The Tx-Rx separation distance and LoS or nLoS conditions for each Tx position are shown in Table 1. Fig. 1 shows the Rx subsystem and the Tx antenna in position 1. To guarantee stationary channel conditions, the measurements were carried out at night, without the presence of people or any moving object.

V. RESULTS

As hinted in Section IV, the amount of collected data is tremendous. To keep the analyzes manageable and also to keep the focus on the 5G bands, the frequencies chosen for investigation were 26, 28 and 39 GHz. All six scenarios, as described in Table 1, were explored.

A. FIRST-ORDER STATISTICS

In the analysis conducted here, the parameters of the target fading models (i.e., Rayleigh, Rice, Nakagami, α-μ, κ-μ, κ-1/2 or FN, κ-3/2, η-μ, and α-η-κ-μ) have been estimated for each one of the frequencies in all considered scenarios. The Matlab least-square-error based function `lsqcurvefit` [29] has been customized and used for parameter estimation purposes. The same method and

$$f_P(\rho) = \frac{\sqrt{\mu}(1+\kappa)^{\frac{1}{4}(2\mu+1)}\rho^{\mu-\frac{1}{2}}}{\sqrt{\pi}\kappa^{\frac{1}{4}(2\mu-1)}\exp\left(\mu(1+\kappa)\left(\rho-\sqrt{\frac{\kappa}{1+\kappa}}\right)^2\right)} \times \sum_{i=0}^{1}\sum_{\ell=0}^{\left\lfloor\frac{2|\mu-1|-1}{4}-\frac{i}{2}\right\rfloor} \frac{(-1)^i\left(|\mu-1|-\frac{1}{2}+2\ell+i\right)!\left(1+(-1)^{i+\frac{1}{2}-\mu}\exp\left(-4\sqrt{\kappa(1+\kappa)}\mu\rho\right)\right)}{(2\ell+i)!\left(|\mu-1|-\frac{1}{2}-2\ell-i\right)!\left(4\mu\rho\sqrt{\kappa(1+\kappa)}\right)^{2\ell+i}} \quad (1)$$

starting point have been utilized for all distributions to keep a fair comparison. After estimating the parameters, the NMSE, the KS as well as the AIC metrics are found.

Tables 2 and 3 show parameter estimates employing the nonlinear least square (LS) method, the values of NMSE, in dB, the KS statistic D, the corresponding p-value, and the AIC statistic for each target distribution. Bold-faced numbers highlight the best-fitting result in each performance metric. From Table 2, it can be seen that the NMSE, KS, and AIC criteria do not necessarily agree with each other, as anticipated. In the first and second criteria, the best-fittings have been achieved by the more general fading distributions in 18 out of 18 tests, through the third metric this result is 16 out of 18. As expected, considering the NMSE and the KS criteria, the more general distributions perform better than the simpler ones since they have more parameters and thus are more flexible. On the other hand, when considering the AIC metric, we find that in some few cases (2 out of 18), the conventional distributions obtained the best compromise solution. As already mentioned and as well known, the AIC penalizes the distributions with a greater number of parameters. However, as can be verified by the results, in most situations (16 of 18) the more general distributions provided an adjustment gain that justifies the increase of complexity. It is important to emphasize that there are several GoF methods in the literature (e.g., Deviance and Bayesian etc.) in addition to those used in this work, each of which focused on a different characteristic and, therefore, may generate different results from those presented here.

In order to exemplify the fitting process results, Fig. 3 depicts theoretical PDFs and CDFs plotted alongside the empirical ones for Scenario 4 and frequency of 28 GHz as a function of normalized envelope in dB. Through a visual analysis of Fig. 3(a), it is possible to verify that, except for the Rayleigh and the FN cases, which are the lower and higher curves at 0 dB, respectively, all the other distributions match rather well the empirical densities. Analyzing the CDF curves in Fig. 3(b), it is possible to notice, again, that the Rayleigh and the FN distributions are unable to follow the tendency of the empirical curve. The η-μ and Nakagami distributions adhere more than the previous ones, but less than the others. All others distributions can visually capture the behavior of empirical CDF, however, if the very lower region of the graph is on focus, the distributions that capture the trend

$$F_P(\rho) = \frac{1}{2\sqrt{\pi}} \sum_{\ell=0}^{1} \sum_{J=0}^{\left\lfloor \frac{2|\mu-1|-1}{4} - \frac{\ell}{2} \right\rfloor} \sum_{i=0}^{\mu-\frac{1}{2}-\ell-2J} \binom{\mu-\frac{1}{2}-\ell-2J}{i} \frac{(-1)^{\ell}\left(|\mu-1|-\frac{1}{2}+2J+\ell\right)!}{(2J+\ell)!\left(|\mu-1|-\frac{1}{2}-2J-\ell\right)!} \frac{(\kappa\mu)^{-\ell-2J-\frac{i}{2}}}{4^{\ell+2J}}$$
$$\times \sum_{n=0}^{1} \operatorname{sign}\left((-1)^{1-n}\left(\rho+(-1)^{n}\sqrt{\frac{\kappa}{1+\kappa}}\right)\right)^{i+n} \Gamma\left(\frac{1+i}{2}, \mu(1+\kappa)\left(\rho-(-1)^{1-n}\sqrt{\frac{\kappa}{1+\kappa}}\right)^{2}\right) \tag{3}$$

$$N_P(\rho) = \frac{(1+\kappa)^{\frac{\mu}{2}-\frac{1}{4}}\sqrt{-\ddot{\psi}(0)}\rho^{\mu-\frac{1}{2}}}{2\pi\kappa^{\frac{1}{4}(2\mu-1)}\exp\left(\mu(1+\kappa)\left(\rho-\sqrt{\frac{\kappa}{1+\kappa}}\right)^{2}\right)}$$
$$\times \sum_{i=0}^{1} \sum_{J=0}^{\left\lfloor \frac{2|\mu-1|-1}{4} - \frac{i}{2} \right\rfloor} \frac{(-1)^{i}\left(|\mu-1|+2J+i-\frac{1}{2}\right)!\left(1+(-1)^{\frac{1}{2}-\mu-i}\exp\left(-4\sqrt{\kappa(1+\kappa)}\mu\rho\right)\right)}{(2J+i)!\left(|\mu-1|-2J-i-\frac{1}{2}\right)!\left(4\mu\rho\sqrt{\kappa(1+\kappa)}\right)^{2J+i}} \tag{4}$$

$$f_P(\rho) = \frac{\sqrt{3}\rho(1+\kappa)}{\sqrt{2\pi\kappa}}\left(1-\exp(-6\rho\sqrt{\kappa(1+\kappa)})\right)\exp\left(-\frac{3(1+\kappa)}{2}\left(\rho-\sqrt{\frac{\kappa}{1+\kappa}}\right)^{2}\right) \tag{5}$$

$$f_P(\rho) = \sqrt{\frac{2(1+\kappa)}{\pi}}\frac{\exp\left(-\frac{1}{2}\left((1+\kappa)\rho^{2}\right)\right)}{\exp(0.5\kappa)}\cosh\left(\sqrt{\kappa(\kappa+1)}\rho\right) \tag{6}$$

$$F_p(\rho) = \frac{\sum_{i=0}^{1}\sum_{n=0}^{1}\operatorname{sign}\left((-1)^{1-n}\left(\rho+(-1)^{n}\sqrt{\frac{\kappa}{1+\kappa}}\right)\right)^{i+n}\Gamma\left(\frac{1+i}{2}, 0, \frac{3(1+\kappa)}{2}\left(\rho-(-1)^{1-n}\sqrt{\frac{\kappa}{1+\kappa}}\right)^{2}\right)\left(\frac{2}{3\kappa}\right)^{\frac{i}{2}}}{2\sqrt{\pi}} \tag{7}$$

$$F_P(\rho) = Q\left(\sqrt{\kappa}-\sqrt{1+\kappa}\rho\right) - Q\left(\sqrt{1+\kappa}\rho+\sqrt{\kappa}\right) \tag{8}$$

$$N_P(\rho) = \frac{\rho\sqrt{1+\kappa}\sqrt{-\ddot{\psi}(0)}}{2\pi\sqrt{\kappa}}\left(1-\exp(-6\rho\sqrt{\kappa(1+\kappa)})\right)\exp\left(-\frac{3(1+\kappa)}{2}\left(-\sqrt{\frac{\kappa}{1+\kappa}}+\rho\right)^{2}\right) \tag{9}$$

$$N_P(\rho) = \frac{\sqrt{-\ddot{\psi}(0)}}{\pi\exp(0.5\kappa)}\exp\left(-\frac{1}{2}\left((1+\kappa)\rho^{2}\right)\right)\cosh\left(\sqrt{\kappa(1+\kappa)}\rho\right) \tag{10}$$

TABLE 2. PDF fitting results for **Scenario 1, Scenario 2, and Scenario 3.**

Scenarios	Frequency	Distribution	$\hat{\alpha}$	$\hat{\eta}$	$\hat{\kappa}$	$\hat{\mu}$	$\hat{p}$	$\hat{q}$	$\hat{\hat{r}}$	NMSE [dB]	KS test		AIC
											D	p-value	
Scenario 1	26 GHz	Rayleigh	-	-	-	-	-	-	1.04	-13.43	0.06	≈ 0	-216.45
		Rice	-	-	1.72	-	-	-	0.98	-30.10	0.01	≈ 0	-406.41
		Nakagami	-	-	-	1.52	-	-	≈ 1	-23.53	0.02	≈ 0	-330.74
		α-μ	2.96	-	-	0.82	-	-	1.04	-27.23	0.02	≈ 0	-371.37
		κ-μ	-	-	1.92	0.95	-	-	0.98	-30.22	0.02	≈ 0	-405.76
		κ-1/2 (FN)	-	-	5.24	-	-	-	0.96	-25.47	0.02	≈ 0	-353.17
		κ-3/2	-	-	0.38	-	-	-	1.00	-24.23	0.02	≈ 0	-338.81
		η-μ	-	≈ 1	-	1.52	-	-	≈ 1	-23.53	0.02	≈ 0	-328.74
		α-η-κ-μ	2.54	1.02	0.84	0.82	0.18	0.17	1.05	**-36.74**	**≈ 0**	**0.85**	**-472.91**
	28 GHz	Rayleigh	-	-	-	-	-	-	1.03	-25.06	0.02	≈ 0	-358.24
		Rice	-	-	0.57	-	-	-	1.01	-31.08	≈ 0	0.09	-425.61
		Nakagami	-	-	-	1.07	-	-	1.02	-27.54	0.01	≈ 0	-384.83
		α-μ	2.51	-	-	0.76	-	-	1.05	-31.63	0.01	0.27	**-429.97**
		κ-μ	-	-	0.70	0.96	-	-	≈ 1	-16.38	**0.01**	**0.42**	-429.05
		κ-1/2 (FN)	-	-	3.57	-	-	-	0.97	-18.54	0.03	≈ 0	-283.51
		κ-3/2	-	-	≈ 0	-	-	-	1.01	-14.54	0.07	≈ 0	-235.21
		η-μ	-	≈ 1	-	1.07	-	-	1.02	-27.54	0.1	≈ 0	-382.83
		α-η-κ-μ	2.23	1.11	0.46	0.87	1.11	1.73	1.02	**-31.81**	0.01	0.30	-423.99
	39 GHz	Rayleigh	-	-	-	-	-	-	1.07	-11.04	0.09	0	-180.46
		Rice	-	-	2.27	-	-	-	≈ 1	-33.96	0.01	0.30	-442.30
		Nakagami	-	-	-	1.80	-	-	1.03	-23.74	0.02	≈ 0	-324.67
		α-μ	3.18	-	-	0.84	-	-	1.07	-31.21	0.01	0.01	-408.60
		κ-μ	-	-	2.39	0.98	-	-	≈ 1	-34.00	0.01	0.38	-440.70
		κ-1/2 (FN)	-	-	6.24	-	-	-	≈ 1	-28.90	0.01	≈ 0	-384.00
		κ-3/2	-	-	0.88	-	-	-	1.02	-28.01	0.02	≈ 0	-373.78
		η-μ	-	≈ 1	-	1.80	-	-	1.03	-23.74	0.02	≈ 0	-322.67
		α-η-κ-μ	2.06	2.24	2.07	≈ 1	2.24	2.05	≈ 1	**-34.12**	**0.001**	**0.70**	**-434.14**
Scenario 2	26 GHz	Rayleigh	-	-	-	-	-	-	1.04	-19.56	0.04	≈ 0	-292.62
		Rice	-	-	0.93	-	-	-	1	-31.51	0.01	0.01	-428.17
		Nakagami	-	-	-	1.18	-	-	1.03	-24.29	0.02	≈ 0	-345.08
		α-μ	2.95	-	-	0.66	-	-	1.07	-32.85	0.01	0.10	-441.56
		κ-μ	-	-	1.20	0.92	-	-	1	-33.09	0.01	0.41	-444.40
		κ-1/2 (FN)	-	-	3.99	-	-	-	0.98	-21.33	0.02	≈ 0	-311.01
		κ-3/2	-	-	≈ 0	-	-	-	1.02	-17.17	0.06	≈ 0	-263.13
		η-μ	-	1	-	1.17	-	-	1.03	-24.29	0.02	≈ 0	-343.08
		α-η-κ-μ	2.90	1.74	0.44	0.66	0.66	0.48	1.07	**-34.12**	**≈ 0**	**0.65**	**-448.22**
	28 GHz	Rayleigh	-	-	-	-	-	-	≈ 1	-26.64	0.02	≈ 0	-385.34
		Rice	-	-	0.50	-	-	-	0.98	-30.25	0.01	≈ 0	-424.84
		Nakagami	-	-	-	1.08	-	-	0.99	-32.79	0.005	0.07	-454.11
		α-μ	2.02	-	-	1.06	-	-	0.99	-32.80	0.006	0.04	-452.22
		κ-μ	-	-	≈ 0	1.08	-	-	0.99	-32.79	0.005	0.07	-452.11
		κ-1/2 (FN)	-	-	3.60	-	-	-	0.93	-17.73	0.04	≈ 0	-280.75
		κ-3/2	-	-	≈ 0	-	-	-	0.97	-14.76	0.06	≈ 0	-246.56
		η-μ	-	1.39	-	1.08	-	-	0.99	-32.90	0.003	0.39	-453.42
		α-η-κ-μ	2.71	0.43	≈ 0	0.74	1.53	0.10	1.07	**-35.47**	**0.002**	**0.99**	**-474.95**
	39 GHz	Rayleigh	-	-	-	-	-	-	1.04	-19.23	0.03	≈ 0	-289.39
		Rice	-	-	0.97	-	-	-	≈ 1	-31.76	0.003	0.58	-431.66
		Nakagami	-	-	-	1.21	-	-	1.02	-26.29	0.01	≈ 0	-368.65
		α-μ	2.64	-	-	0.79	-	-	1.05	-31	0.004	0.36	-420.94
		κ-μ	-	-	0.97	1	-	-	≈ 1	-31.76	0.003	0.56	-429.66
		κ-1/2 (FN)	-	-	4.09	-	-	-	0.97	-20.72	0.02	≈ 0	-304.54
		κ-3/2	-	-	≈ 0	-	-	-	1.01	-18.22	0.05	≈ 0	-275.73
		η-μ	-	≈ 1	-	1.21	-	-	1.02	-26.29	0.01	≈ 0	-366.64
		α-η-κ-μ	3.10	0.10	0.43	0.63	0.51	2.81	1.08	**-32.75**	**0.003**	**0.78**	**-433.08**
Scenario 3	26 GHz	Rayleigh	-	-	-	-	-	-	1.01	-28.61	0.01	≈ 0	-410.83
		Rice	-	-	0.37	-	-	-	≈ 1	-30.63	0.007	≈ 0	-432.16
		Nakagami	-	-	-	1.02	-	-	≈ 1	-28.88	0.01	≈ 0	-411.99
		α-μ	2.40	-	-	0.78	-	-	1.03	-32.23	0.005	0.08	-448.58
		κ-μ	-	-	0.60	0.94	-	-	0.99	-32.38	**0.004**	**0.15**	**-450.31**
		κ-1/2 (FN)	-	-	3.36	-	-	-	0.95	-18.21	0.03	≈ 0	-289.19
		κ-3/2	-	-	≈ 0	-	-	-	0.99	-13.28	0.08	≈ 0	-232.37
		η-μ	-	≈ 1	-	1.02	-	-	≈ 1	-28.88	0.01	≈ 0	-409.99
		α-η-κ-μ	2.13	1.12	0.45	0.89	1.15	1.33	1	**-32.49**	0.005	0.08	-443.59
	28 GHz	Rayleigh	-	-	-	-	-	-	1.02	-27.10	0.02	≈ 0	-384.08
		Rice	-	-	0.51	-	-	-	≈ 1	-33.60	0.003	0.39	-456.95
		Nakagami	-	-	-	1.06	-	-	1.02	-30.81	0.01	≈ 0	-424.75
		α-μ	2.30	-	-	0.86	-	-	1.03	-33.72	0.003	0.45	-456.36
		κ-μ	-	-	0.51	≈ 1	-	-	≈ 1	-33.60	0.003	0.40	-454.96
		κ-1/2 (FN)	-	-	3.54	-	-	-	0.96	-18.32	0.03	≈ 0	-280.96
		κ-3/2	-	-	≈ 0	-	-	-	1.00	-14.46	0.07	≈ 0	-236.57
		η-μ	-	≈ 1	-	1.06	-	-	1.02	-30.81	0.1	≈ 0	-422.75
		α-η-κ-μ	2.81	2.39	1.01	0.68	0.69	2.70	1.07	**-34.69**	**0.002**	**0.98**	**-459.53**
	39 GHz	Rayleigh	-	-	-	-	-	-	≈ 1	-35.82	0.003	0.26	-493.57
		Rice	-	-	≈ 0	-	-	-	≈ 1	-35.82	0.004	0.26	-491.57
		Nakagami	-	-	-	0.99	-	-	≈ 1	-36.84	0.002	0.86	**-503.40**
		α-μ	2.02	-	-	0.97	-	-	≈ 1	-36.91	0.002	0.92	-502.11
		κ-μ	-	-	0.14	0.98	-	-	≈ 1	-36.96	**0.002**	**0.94**	-502.71
		κ-1/2 (FN)	-	-	3.23	-	-	-	0.94	-16.97	0.04	≈ 0	-274.56
		κ-3/2	-	-	≈ 0	-	-	-	0.97	-12.58	0.08	≈ 0	-224.00
		η-μ	-	≈ 1	-	0.99	-	-	≈ 1	-36.84	0.002	0.86	-501.40
		α-η-κ-μ	1.85	1.26	0.38	1.07	1.25	1.37	0.98	**-37.04**	0.002	0.93	-495.70

TABLE 3. PDF fitting results for **Scenario 4, Scenario 5, and Scenario 6.**

Scenarios	Frequency	Distribution	$\hat{\alpha}$	$\hat{\eta}$	$\hat{\kappa}$	$\hat{\mu}$	$\hat{p}$	$\hat{q}$	$\hat{\hat{r}}$	NMSE [dB]	KS test		AIC
											D	p-value	
Scenario 4	26 GHz	Rayleigh	-	-	-	-	-	-	1.05	−15.58	0.05	≈ 0	−243.03
		Rice	-	-	1.37	-	-	-	≈ 1	−32.79	0.005	0.06	−439.13
		Nakagami	-	-	-	1.37	-	-	1.02	−25.48	0.02	≈ 0	−354.97
		α-μ	2.81	-	-	0.80	-	-	1.05	−31.41	0.006	0.01	−421.27
		κ-μ	-	-	1.24	1.04	-	-	≈ 1	−32.99	0.004	0.18	−439.48
		κ-1/2 (FN)	-	-	4.69	-	-	-	0.97	−22.95	0.02	≈ 0	−325.84
		κ-3/2	-	-	≈ 0	-	-	-	1.02	−23.02	0.03	≈ 0	−326.73
		η-μ	-	≈ 1	-	1.37	-	-	1.02	−25.48	0.02	≈ 0	−352.97
		α-η-κ-μ	3.40	0.72	0.56	0.63	2.40	0.71	1.10	**−34.28**	**≈ 0**	**0.94**	**−446.33**
	28 GHz	Rayleigh	-	-	-	-	-	-	1.04	−19.57	0.03	≈ 0	−288.70
		Rice	-	-	0.94	-	-	-	≈ 1	−32.39	0.003	0.55	−434.29
		Nakagami	-	-	-	1.20	-	-	1.03	−26.80	0.01	≈ 0	−369.99
		α-μ	2.65	-	-	0.78	-	-	1.06	−32.84	0.002	0.89	**−437.44**
		κ-μ	-	-	0.87	1.02	-	-	≈ 1	−32.51	0.003	0.26	−433.70
		κ-1/2 (FN)	-	-	4.05	-	-	-	0.98	−20.20	0.03	≈ 0	−293.99
		κ-3/2	-	-	≈ 0	-	-	-	1.02	−17.94	0.05	≈ 0	−267.94
		η-μ	-	≈ 1	-	1.20	-	-	1.03	−26.80	0.02	≈ 0	−367.99
		α-η-κ-μ	2.57	0.49	1.70	0.78	1.58	0.31	1.05	**−33.23**	**0.002**	**0.97**	−433.95
	39 GHz	Rayleigh	-	-	-	-	-	-	1.03	−21.59	0.02	≈ 0	−315.73
		Rice	-	-	0.79	-	-	-	≈ 1	−30.58	0.006	≈ 0	−417.13
		Nakagami	-	-	-	1.16	-	-	1.02	−30.45	0.01	≈ 0	−415.69
		α-μ	2.28	-	-	0.94	-	-	1.03	−32.58	0.005	0.08	−438.23
		κ-μ	-	-	0.49	1.09	-	-	≈ 1	−32.43	0.005	0.07	−436.45
		κ-1/2 (FN)	-	-	3.89	-	-	-	0.97	−18.83	0.03	≈ 0	−281.94
		κ-3/2	-	-	≈ 0	-	-	-	1.01	−16.91	0.05	≈ 0	−259.79
		η-μ	-	≈ 1	-	1.16	-	-	1.02	−30.45	0.01	≈ 0	−413.69
		α-η-κ-μ	3.29	2.07	0.99	0.62	0.55	4.64	1.10	**−34.99**	**0.002**	**0.97**	**−458**
Scenario 5	26 GHz	Rayleigh	-	-	-	-	-	-	1.04	−15.28	0.05	≈ 0	−239.66
		Rice	-	-	1.41	-	-	-	0.99	−31.95	0.008	≈ 0	−429.50
		Nakagami	-	-	-	1.39	-	-	1.02	−25.90	0.02	≈ 0	−359.90
		α-μ	2.71	-	-	0.86	-	-	1.04	−30.40	0.007	≈ 0	−406.72
		κ-μ	-	-	1.21	1.06	-	-	0.99	−32.32	0.006	≈ 0	−431.77
		κ-1/2 (FN)	-	-	4.75	-	-	-	0.97	−23.02	0.02	≈ 0	−326.79
		κ-3/2	-	-	≈ 0	-	-	-	1.01	−23.93	0.03	≈ 0	−337.23
		η-μ	-	≈ 1	-	1.39	-	-	1.02	−25.90	0.02	≈ 0	−357.90
		α-η-κ-μ	2.40	0.40	0.91	0.86	1.12	2.35	1.03	**−34.21**	**0.002**	**0.85**	**−445.61**
	28 GHz	Rayleigh	-	-	-	-	-	-	1.06	−10.22	0.10	0	−174.94
		Rice	-	-	2.56	-	-	-	0.99	−33.45	0.006	0.009	−440.32
		Nakagami	-	-	-	1.94	-	-	1.02	−24.25	0.02	≈ 0	−334.49
		α-μ	3.05	-	-	0.96	-	-	1.05	−29.16	0.009	≈ 0	−388.95
		κ-μ	-	-	2.82	0.94	-	-	0.99	−33.52	0.007	≈ 0	−439.14
		κ-1/2 (FN)	-	-	6.77	-	-	-	0.99	−30.58	0.01	≈ 0	−407.38
		κ-3/2	-	-	1.09	-	-	-	1.01	−29.16	0.01	≈ 0	−390.99
		η-μ	-	≈ 1	-	1.94	-	-	1.02	−24.25	0.02	≈ 0	−332.49
		α-η-κ-μ	2.40	1.11	1.57	0.92	3.20	2.88	1.02	**−35.50**	**0.002**	**0.99**	**−453.98**
	39 GHz	Rayleigh	-	-	-	-	-	-	1.04	−15.37	0.05	≈ 0	−242.99
		Rice	-	-	1.40	-	-	-	0.99	−32.08	0.008	≈ 0	−433.27
		Nakagami	-	-	-	1.38	-	-	1.02	−24.92	0.02	≈ 0	−350.88
		α-μ	2.80	-	-	0.81	-	-	1.05	−29.38	0.008	≈ 0	−400.25
		κ-μ	-	-	1.42	0.99	-	-	0.99	−32.08	0.008	≈ 0	−431.31
		κ-1/2 (FN)	-	-	4.71	-	-	-	0.97	−23.84	0.02	≈ 0	−338.41
		κ-3/2	-	-	≈ 0	-	-	-	1.01	−23.08	0.03	≈ 0	−329.70
		η-μ	-	≈ 1	-	1.38	-	-	1.02	−24.92	0.02	≈ 0	−348.88
		α-η-κ-μ	2.32	1.41	1.02	0.85	0.49	0.36	1.03	**−34.73**	**0.001**	**0.99**	**−453.83**
Scenario 6	26 GHz	Rayleigh	-	-	-	-	-	-	1.05	−16.27	0.05	≈ 0	−250.91
		Rice	-	-	1.28	-	-	-	≈ 1	−31.89	0.006	≈ 0	−428.77
		Nakagami	-	-	-	1.34	-	-	1.03	−27.49	0.01	≈ 0	−378.10
		α-μ	2.59	-	-	0.89	-	-	1.05	−32.64	0.004	0.13	−435.44
		κ-μ	-	-	0.94	1.11	-	-	1	−33.39	0.003	0.30	−444.09
		κ-1/2 (FN)	-	-	4.57	-	-	-	0.98	−21.69	0.02	≈ 0	−311.38
		κ-3/2	-	-	≈ 0	-	-	-	1.02	−22.80	0.03	≈ 0	−324.15
		η-μ	-	≈ 1	-	1.34	-	-	1.03	−27.49	0.01	≈ 0	−376.10
		α-η-κ-μ	2.67	2.26	1.59	0.78	0.64	1.62	1.05	**−35.73**	**0.002**	**0.99**	**−462.95**
	28 GHz	Rayleigh	-	-	-	-	-	-	1.05	−16.15	0.05	≈ 0	−249.80
		Rice	-	-	1.29	-	-	-	≈ 1	−33.09	0.004	0.24	−442.88
		Nakagami	-	-	-	1.33	-	-	1.03	−23.91	0.02	≈ 0	−337.20
		α-μ	3.00	-	-	0.71	-	-	1.07	−31.19	0.004	0.09	−419.04
		κ-μ	-	-	1.50	0.94	-	-	1	−33.73	0.002	0.93	**−448.29**
		κ-1/2 (FN)	-	-	4.52	-	-	-	0.98	−23.52	0.02	≈ 0	−332.69
		κ-3/2	-	-	≈ 0	-	-	-	1.03	−21.10	0.04	≈ 0	−304.88
		η-μ	-	≈ 1	-	1.33	-	-	1.03	−23.91	0.02	≈ 0	−335.20
		α-η-κ-μ	2.59	0.62	1.45	0.75	1.58	0.70	1.05	**−33.93**	**0.002**	**0.99**	−442.59
	39 GHz	Rayleigh	-	-	-	-	-	-	1.05	−16.46	0.04	≈ 0	−255.41
		Rice	-	-	1.25	-	-	-	≈ 1	−35.30	0.002	0.81	**−470.31**
		Nakagami	-	-	-	1.32	-	-	1.03	−25.12	0.02	≈ 0	−353.12
		α-μ	2.88	-	-	0.75	-	-	1.06	−33.26	0.003	0.29	−444.78
		κ-μ	-	-	1.29	0.99	-	-	≈ 1	−35.33	0.002	0.92	−469.67
		κ-1/2 (FN)	-	-	4.49	-	-	-	0.98	−22.86	0.02	≈ 0	−327.12
		κ-3/2	-	-	≈ 0	-	-	-	1.03	−21.34	0.04	≈ 0	−309.53
		η-μ	-	≈ 1	-	1.32	-	-	1.03	−25.12	0.02	≈ 0	−351.12
		α-η-κ-μ	2.21	2.47	1.57	0.89	1.15	1.66	1.02	**−35.41**	**0.002**	**0.94**	−461.59

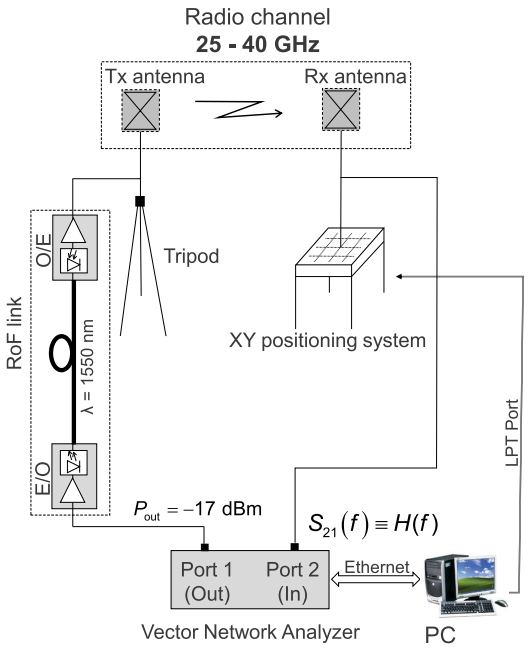

FIGURE 2. **Schematic diagram of the channel sounder.**

of empirical lower tail CDF are α-η-κ-μ and α-μ distributions. In fact, in this particular case, through the objective statistical measure, the α-η-κ-μ distribution is selected as the one yielding the best-fitting considering the NMSE and the KS metrics while for AIC metric the selected one is the α-μ distribution. Through the previously presented results, an important conclusion can be reached. The behavior of the communication channel can be characterized by different combinations of physical phenomena (i.e. non-linearity of the medium, multipath clustering, dominant signal power, among others). Therefore, it is practically impossible to have a single combination of distributions parameters that will categorically describe the channel. In general, the environments are rather complex and there is no single or simple solution either in physical or mathematical terms in channel modeling [21].

B. SECOND-ORDER STATISTICS

At this point, second order statistics are evaluated using the same methodology already presented for first order analyzes with exception of KS test, that only applies to the PDF curves. The adherence of the theoretical LCR curves to the empirical LCR ones in all six scenarios described in Section IV is assessed.

Tables 4 and 5 summarize the parameter estimates and the values of NMSE in dB and AIC. The parameter $\ddot{\psi}(0)$[1] denotes the mean of the second derivative with respect to time/distance of the autocorrelation function at zero. Based on the aforementioned tables, it can be seen that in all six evaluated scenarios a better fitting performance has been achieved by the more general fading models. If we consider both metrics in the six analyzed scenarios and for the three considered frequencies, the best performance has been achieved by the α-η-κ-μ, i.e. in 18 out of 18 tests. This reveals that the increase in complexity for the α-η-κ-μ distribution, due to the greater number of parameters, is rewarded by a much better adjustment than those of the simpler distributions, thus justifying its use in situations where a refined modeling is desired for LCR.

[1] As can be seen in [22], $\ddot{\psi}(0)$ is the second derivative with respect to space of the spatial autocorrelation function at zero. Such a parameter arises from the underlying Gaussian process composing the fading models. Because such a parameter appears as a multiplicative factor in the concerned expressions, for the application at hand, the knowledge of the proper autocorrelation function is irrelevant, for the parameter can be obtained in the curve fitting process as any other parameter. But, of course, if one is interested in knowing the true autocorrelation function, a physical fading model can be envisaged to take into account the relevant phenomena, as was the case for the Clarke's (Jake's) model.

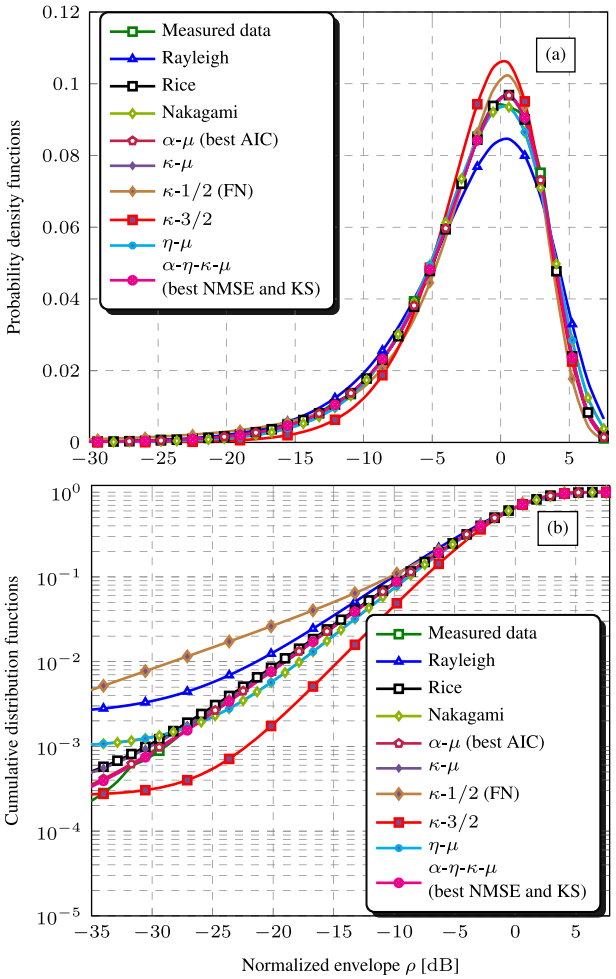

FIGURE 3. **Estimated and theoretical (a) PDFs and (b) CDFs for Scenario 4 at 28 GHz. This figure is better viewed in color.**

In order to exemplify the LCR fitting process, Fig. 4 shows theoretical LCR curves plotted alongside the empirical one for all six scenarios at frequency 28 GHz as a function of ρ in dB. Through a visual inspection, it is possible to verify that, for all presented curves in Fig. 4, for $\rho > -15$ dB all distributions match rather well the empirical LCR. It can also be seen that for $\rho < -15$ dB, for severe fading conditions, Rayleigh, Rice and FN models are unable to adhere well to the empirical

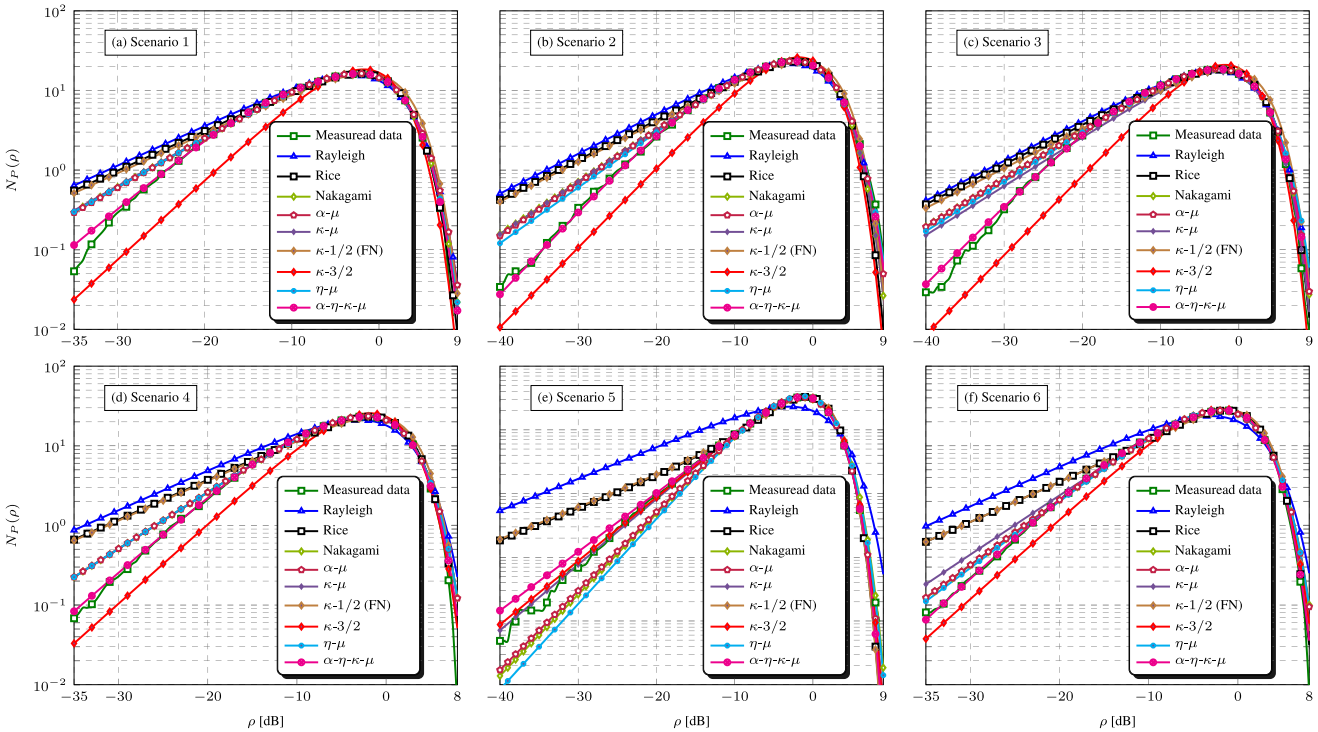

FIGURE 4. LCR fitting approach for Scenarios 1 (a), 2 (b), 3 (c), 4 (d), 5 (e) and 6 (f) at frequency 28 GHz. This figure is better viewed in color.

curves. The second group of theoretical distributions that provides an intermediate tail adhesion comprises Nakagami, κ-μ, η-μ, and α-μ. However, if we verify only the extremely lower tail portion of the plots, i.e., for substantially small ρ, the α-η-κ-μ yielded a better adherence except in Scenario 5, where the κ-μ model achieved the best tail adherence. In other scenarios, the distribution that achieved the best values for the NMSE metric will also have the best tail adjustment.

C. FIRST AND SECOND ORDER STATISTICS ANALYSES

The Rayleigh distribution showed low performance in LoS scenarios, as expected, since its physical model does not include dominant components. However, in nLoS scenarios, and if high fitting accuracy is not required, its performance is remarkable, bearing in mind its simple and elegant functional form. The simplest forms of the κ-μ model, namely κ-1/2 (FN) and κ-3/2, can be useful for a quick performance evaluation. However, they fail to yield good fitting performance mainly in nLoS conditions. The Rice distribution showed satisfactory results in LoS scenarios, as expected, and surprisingly, it also operated reasonably well in nLoS situations (Scenario 3), in which case its κ factor is found to be very low as compared to those of the LoS cases. The Nakagami distribution, despite having only one parameter in its physical model, achieved interesting results in LoS conditions, although its physical model does not consider dominant components, which is somehow emulated by the clustering effect. Another distribution that does not provide dominant components in its modeling, but which performs very satisfactorily, both in LoS and nLoS scenarios, is the α-μ. In this case, in addition to the clustering effect, the provision for the nonlinearity of the medium yields further flexibility for data adjustment. Because the majority of the scenarios under investigation are in the LoS situation (5 out of 6), the κ-μ distribution performed better than the α-μ in most cases, showing excellent results of adjustments, losing only to a more generalized distribution, namely α-η-κ-μ. Of course, its great advantage is its relative simplicity, comparable to that of Rice. The η-μ distribution, although in some situations yielded results comparable to those of α-μ and κ-μ, failed to maintain the regularity in all situations. Finally, the α-η-κ-μ distribution presented the best fit, in terms of mean square errors, in all situations, both for PDF and for LCR. As understood from its physical model, it can combine, in a very powerful way, the most relevant propagation phenomena. Impressively, the α-η-κ-μ distribution provided a reduction of the mean square error of more than 15 dB concerning the second-best distribution in some cases of LCR evaluation. Of course, its remarkable performance comes at the expenses of its more complex formulation, which is a result of its more comprehensive physical modeling

An important conclusion is due. There is no single combination of physical phenomena that will categorically describe the behavior of the communication channel. Different combinations of physical phenomena, such as medium nonlinearity, multipath clustering, presence/absence of dominant components, among others, can result in similar performance.

TABLE 4. LCR fitting results for Scenario 1, Scenario 2, and Scenario 3.

Scenarios	Frequency	Distribution	$\hat{\alpha}$	$\hat{\eta}$	$\hat{\kappa}$	$\hat{\mu}$	$\hat{p}$	$\hat{q}$	$\hat{d}$	$\hat{\psi}[\times 10^3]$	NMSE [dB]	AIC
Scenario 1	26 GHz	Rayleigh	-	-	-	-	-	-	-	-1.94	-11.49	74.14
		Rice	-	-	1.64	-	-	-	-	-5.98	-25.12	-253.35
		Nakagami	-	-	-	1.42	-	-	-	-3.09	-23.48	-213.60
		α-μ	2.03	-	-	1.39	-	-	-	-3.10	-23.50	-212.09
		κ-μ	-	-	0.98	1.19	-	-	-	-5.28	-29.34	-353.42
		κ-1/2 (FN)	-	-	4.48	-	-	-	-	-6.88	-22.26	-182.07
		κ-3/2	-	-	0.04	-	-	-	-	-3.39	-22.34	-186.15
		η-μ	-	2.38	-	1.42	-	-	-	-3.10	-23.48	-211.56
		α-η-κ-μ	1.65	1.07	6.70	1.48	4.03	≈ 0	9.42	-6.91	$\mathbf{-34.36}$	$\mathbf{-464.61}$
	28 GHz	Rayleigh	-	-	-	-	-	-	-	-4.08	-19.24	-50.39
		Rice	-	-	0.72	-	-	-	-	-7.44	-23.39	-154.30
		Nakagami	-	-	-	1.12	-	-	-	-4.77	-28.45	-283.76
		α-μ	1.92	-	-	1.15	-	-	-	-4.75	-28.83	-291.34
		κ-μ	-	-	0.17	1.11	-	-	-	-5.57	-28.55	-284.25
		κ-1/2 (FN)	-	-	2.22	-	-	-	-	-1.06	-19.27	-47.08
		κ-3/2	-	-	≈ 0	-	-	-	-	-6.17	-13.06	109.64
		η-μ	-	0.99	-	0.56	-	-	-	-4.80	-28.44	-281.43
		α-η-κ-μ	1.59	0.40	2.88	1.65	1.69	≈ 0	8.55	-85.44	$\mathbf{-40.36}$	$\mathbf{-576.23}$
	39 GHz	Rayleigh	-	-	-	-	-	-	-	-4.33	-8.09	266.26
		Rice	-	-	2.46	-	-	-	-	-18.77	-30.60	-338.67
		Nakagami	-	-	-	1.81	-	-	-	-9.35	-19.70	-44.53
		α-μ	1.77	-	-	2.07	-	-	-	-9.21	-20.19	-55.97
		κ-μ	-	-	1.99	1.11	-	-	-	-18.07	-32.19	-379.13
		κ-1/2 (FN)	-	-	6.33	-	-	-	-	-20.69	-30.32	-328.83
		κ-3/2	-	-	0.97	-	-	-	-	-15.68	-25.04	-188.40
		η-μ	-	5.89×10^6	-	1.81	-	-	-	-9.35	-19.70	-42.53
		α-η-κ-μ	2.05	0.29	5.33	1.46	2.61	≈ 0	0.86	-17.94	$\mathbf{-41.38}$	$\mathbf{-616.78}$
Scenario 2	26 GHz	Rayleigh	-	-	-	-	-	-	-	-5.25	-14.66	97.86
		Rice	-	-	1.17	-	-	-	-	-12.74	-24.91	-152.65
		Nakagami	-	-	-	1.24	-	-	-	-7.01	-24.50	-142.52
		α-μ	1.81	-	-	1.34	-	-	-	-6.92	-25.51	-165.53
		κ-μ	-	-	0.70	1.13	-	-	-	-11.16	-29.55	-265.08
		κ-1/2 (FN)	-	-	3.20	-	-	-	-	-15.37	-23.12	-106.62
		κ-3/2	-	-	≈ 0	-	-	-	-	-8.36	-16.61	51.68
		η-μ	-	≈ 1	-	0.63	-	-	-	-7.32	-24.15	-131.95
		α-η-κ-μ	1.72	0.31	2.77	1.56	1.43	≈ 0	5.01	-92.62	$\mathbf{-42.94}$	$\mathbf{-584.91}$
	28 GHz	Rayleigh	-	-	-	-	-	-	-	-8.06	-17.35	70.13
		Rice	-	-	0.80	-	-	-	-	-15.57	-20.74	-22.28
		Nakagami	-	-	-	1.16	-	-	-	-9.85	-28.45	-237.07
		α-μ	1.90	-	-	1.20	-	-	-	-9.78	-29.04	-251.52
		κ-μ	-	-	≈ 0	1.16	-	-	-	-9.85	-28.45	-235.07
		κ-1/2 (FN)	-	-	2.34	-	-	-	-	-21.16	-18.24	49.45
		κ-3/2	-	-	≈ 0	-	-	-	-	-12.39	-14.00	165.405
		η-μ	-	2.48	-	0.60	-	-	-	-9.53	-30.13	-282.03
		α-η-κ-μ	1.39	1.44	3.69	2.00	4.76	≈ 0	12.82	-109.98	$\mathbf{-40.60}$	$\mathbf{-563.80}$
	39 GHz	Rayleigh	-	-	-	-	-	-	-	-11.51	-13.48	222.56
		Rice	-	-	1.28	-	-	-	-	-29.54	-21.35	10.08
		Nakagami	-	-	-	1.29	-	-	-	-16.28	-30.24	-234.59
		α-μ	1.91	-	-	1.34	-	-	-	-16.18	-30.99	-253.08
		κ-μ	-	-	0.36	1.25	-	-	-	-21.60	-32.02	-281.26
		κ-1/2 (FN)	-	-	3.52	-	-	-	-	-35.16	-19.67	57.13
		κ-3/2	-	-	≈ 0	-	-	-	-	-18.69	-19.00	73.22
		η-μ	-	≈ 1	-	0.65	-	-	-	-16.50	-30.11	-228.93
		α-η-κ-μ	1.65	0.94	3.38	1.78	3.22	≈ 0	5.37	-159.83	$\mathbf{-43.68}$	$\mathbf{-590.86}$
Scenario 3	26 GHz	Rayleigh	-	-	-	-	-	-	-	-4.75	-20.48	-72.22
		Rice	-	-	0.62	-	-	-	-	-8.09	-23.79	-157.93
		Nakagami	-	-	-	1.10	-	-	-	-5.38	-27.12	-246.08
		α-μ	1.87	-	-	1.15	-	-	-	-5.34	-28.00	-267.22
		κ-μ	-	-	0.18	1.09	-	-	-	-6.32	-27.21	-246.39
		κ-1/2 (FN)	-	-	2.05	-	-	-	-	-12.22	-19.21	-34.59
		κ-3/2	-	-	≈ 0	-	-	-	-	-7.08	-12.32	145.85
		η-μ	-	≈ 1	-	0.55	-	-	-	-5.38	-27.12	-244.08
		α-η-κ-μ	1.59	1.25	3.91	1.62	4.48	≈ 0	6.02	-57.02	$\mathbf{-40.63}$	$\mathbf{-591.88}$
	28 GHz	Rayleigh	-	-	-	-	-	-	-	-5.37	-20.29	-68.34
		Rice	-	-	0.59	-	-	-	-	-8.96	-22.62	-133.37
		Nakagami	-	-	-	1.10	-	-	-	-6.13	-28.14	-292.27
		α-μ	1.99	-	-	1.11	-	-	-	-6.12	-28.15	-290.58
		κ-μ	-	-	0.24	1.12	-	-	-	-6.30	-18.98	-302.79
		κ-1/2 (FN)	-	-	2.10	-	-	-	-	-13.79	-17.89	4.62
		κ-3/2	-	-	≈ 0	-	-	-	-	-8.04	-12.42	160.21
		η-μ	-	2.03	-	0.56	-	-	-	-6.00	-28.66	-305.31
		α-η-κ-μ	1.47	0.92	4.03	1.84	3.66	≈ 0	14.38	-108.40	$\mathbf{-41.61}$	$\mathbf{-668.00}$
	39 GHz	Rayleigh	-	-	-	-	-	-	-	-16.31	-16.84	171.82
		Rice	-	-	0.73	-	-	-	-	-30.03	-18.74	118.33
		Nakagami	-	-	-	1.15	-	-	-	-19.90	-24.61	-53.12
		α-μ	1.94	-	-	1.18	-	-	-	-19.82	-24.68	-53.25
		κ-μ	-	-	0.41	1.21	-	-	-	-21.34	-14.61	-118.50
		κ-1/2 (FN)	-	-	2.26	-	-	-	-	-42.41	-16.57	183.71
		κ-3/2	-	-	≈ 0	-	-	-	-	-25.00	-13.54	270.50
		η-μ	-	0.19	-	0.65	-	-	-	-18.17	-30.69	-228.95
		α-η-κ-μ	1.54	0.44	1.67	1.84	1.40	≈ 0	7.54	-177.49	$\mathbf{-46.08}$	$\mathbf{-669.15}$

TABLE 5. LCR fitting results for Scenario 4, Scenario 5, and Scenario 6.

Scenarios	Frequency	Distribution	$\hat{\alpha}$	$\hat{\eta}$	$\hat{\kappa}$	$\hat{\mu}$	$\hat{p}$	$\hat{q}$	$\hat{d}$	$\hat{\psi}[\times 10^3]$	NMSE [dB]	AIC
Scenario 4	26 GHz	Rayleigh	-	-	-	-	-	-	-	−6.20	−13.05	160.94
		Rice	-	-	1.37	-	-	-	-	−16.69	−22.47	−91.02
		Nakagami	-	-	-	1.32	-	-	-	−9.02	−29.88	−290.61
		α-μ	2.03	-	-	1.30	-	-	-	−9.04	−29.97	−291.07
		κ-μ	-	-	0.48	1.25	-	-	-	−12.80	−33.80	−394.24
		κ-1/2 (FN)	-	-	3.79	-	-	-	-	−19.70	−20.14	−26.18
		κ-3/2	-	-	≈ 0	-	-	-	-	−10.16	−20.43	−35.98
		η-μ	-	1.01	-	0.66	-	-	-	−9.20	−29.61	−281.38
		α-η-κ-μ	1.67	1.21	4.17	1.55	3.54	≈ 0	6.61	−98.64	**−40.85**	**−574.06**
	28 GHz	Rayleigh	-	-	-	-	-	-	-	−7.57	−15.37	119.08
		Rice	-	-	1.03	-	-	-	-	−16.84	−20.66	−21.26
		Nakagami	-	-	-	1.21	-	-	-	−9.89	−30.47	−285.59
		α-μ	≈ 2	-	-	1.21	-	-	-	−9.89	−30.47	−283.62
		κ-μ	-	-	≈ 0	1.21	-	-	-	−9.89	−30.47	−283.59
		κ-1/2 (FN)	-	-	2.93	-	-	-	-	−21.18	−18.45	40.15
		κ-3/2	-	-	≈ 0	-	-	-	-	−11.95	−16.03	103.53
		η-μ	-	≈ 1	-	0.61	-	-	-	−9.90	−30.47	−283.58
		α-η-κ-μ	1.68	1.39	3.44	1.66	4.31	≈ 0	5.46	−82.88	**−40.49**	**−543.65**
	39 GHz	Rayleigh	-	-	-	-	-	-	-	−10.18	−14.44	183.92
		Rice	-	-	1.13	-	-	-	-	−24.04	−20.40	13.97
		Nakagami	-	-	-	1.25	-	-	-	−13.79	−31.53	−306.45
		α-μ	1.91	-	-	1.29	-	-	-	−13.70	−32.73	−338.94
		κ-μ	-	-	0.09	1.24	-	-	-	−15.05	−31.56	−305.19
		κ-1/2 (FN)	-	-	3.13	-	-	-	-	−29.35	−18.77	62.86
		κ-3/2	-	-	≈ 0	-	-	-	-	−16.28	−17.26	104.15
		η-μ	-	1.33	-	0.63	-	-	-	−13.74	−31.56	−305.39
		α-η-κ-μ	1.52	1.48	3.42	1.87	4.42	≈ 0	6.75	−119.17	**−39.86**	**−534.08**
Scenario 5	26 GHz	Rayleigh	-	-	-	-	-	-	-	−13.18	−11.35	272.51
		Rice	-	-	1.59	-	-	-	-	−39.72	−20.01	73.03
		Nakagami	-	-	-	1.41	-	-	-	−21.05	−33.59	−242.77
		α-μ	2.03	-	-	1.39	-	-	-	−21.09	−33.72	−243.85
		κ-μ	-	-	0.22	1.39	-	-	-	−25.44	−34.14	−253.55
		κ-1/2 (FN)	-	-	4.36	-	-	-	-	−45.79	−18.56	108.82
		κ-3/2	-	-	≈ 0	-	-	-	-	−22.29	−26.49	−77.62
		η-μ	-	≈ 1	-	0.71	-	-	-	−21.27	−33.42	−236.78
		α-η-κ-μ	1.62	0.91	3.62	2.04	3.27	≈ 0	8.04	−277.65	**−42.22**	**−431.44**
	28 GHz	Rayleigh	-	-	-	-	-	-	-	−9.12	−8.17	318.25
		Rice	-	-	2.41	-	-	-	-	−38.80	−22.65	−16.47
		Nakagami	-	-	-	1.78	-	-	-	−19.54	−26.01	−94.59
		α-μ	2.13	-	-	1.67	-	-	-	−19.72	−26.55	−105.29
		κ-μ	-	-	0.77	1.53	-	-	-	−30.42	−29.15	−165.80
		κ-1/2 (FN)	-	-	6.29	-	-	-	-	−42.95	−20.93	25.49
		κ-3/2	-	-	0.84	-	-	-	-	−31.01	−29.10	−166.57
		η-μ	-	0.99	-	0.92	-	-	-	−21.35	−24.15	−49.47
		α-η-κ-μ	2.94	1.46	0.63	1.13	5.72	1.77	0.21	−33.70	**−44.06**	**−502.37**
	39 GHz	Rayleigh	-	-	-	-	-	-	-	−22.35	−10.40	349.74
		Rice	-	-	1.79	-	-	-	-	−73.79	−20.76	110.99
		Nakagami	-	-	-	1.49	-	-	-	−38.34	−34.56	−210.09
		α-μ	1.98	-	-	1.50	-	-	-	−38.28	−34.66	−210.37
		κ-μ	-	-	0.36	1.43	-	-	-	−50.67	−40.00	−334.59
		κ-1/2 (FN)	-	-	4.82	-	-	-	-	−83.81	−19.31	146.51
		κ-3/2	-	-	0.13	-	-	-	-	−43.58	−34.55	−209.90
		η-μ	-	≈ 1	-	0.75	-	-	-	−38.90	−34.15	−198.45
		α-η-κ-μ	2.02	0.85	0.29	1.41	0.46	≈ 0	0.84	−46.49	**−40.87**	**−344.77**
Scenario 6	26 GHz	Rayleigh	-	-	-	-	-	-	-	−5.77	−12.30	177.84
		Rice	-	-	1.47	-	-	-	-	−16.40	−22.93	−131.20
		Nakagami	-	-	-	1.35	-	-	-	−8.72	−27.93	−277.16
		α-μ	1.89	-	-	1.42	-	-	-	−8.65	−28.60	−294.80
		κ-μ	-	-	0.60	1.25	-	-	-	−13.08	−34.59	−469.99
		κ-1/2 (FN)	-	-	4.02	-	-	-	-	−19.06	−21.17	−77.67
		κ-3/2	-	-	≈ 0	-	-	-	-	−9.57	−21.96	−102.80
		η-μ	-	0.97	-	0.68	-	-	-	−8.88	−27.77	−270.50
		α-η-κ-μ	1.54	0.75	4.19	1.79	2.73	≈ 0	8.07	−139.81	**−37.72**	**−551.64**
	28 GHz	Rayleigh	-	-	-	-	-	-	-	−9.49	−12.82	206.57
		Rice	-	-	1.39	-	-	-	-	−25.87	−22.20	−18.23
		Nakagami	-	-	-	1.32	-	-	-	−13.91	−28.26	−164.81
		α-μ	2.01	-	-	1.32	-	-	-	−13.92	−28.27	−163.01
		κ-μ	-	-	0.51	1.25	-	-	-	−20.09	−31.70	−245.92
		κ-1/2 (FN)	-	-	3.86	-	-	-	-	−30.45	−20.14	33.57
		κ-3/2	-	-	≈ 0	-	-	-	-	−15.59	−20.51	22.65
		η-μ	-	≈ 1	-	0.67	-	-	-	−14.47	−27.56	−145.82
		α-η-κ-μ	1.72	0.81	3.98	1.71	3.08	≈ 0	6.35	−189.53	**−44.92**	**−555.39**
	39 GHz	Rayleigh	-	-	-	-	-	-	-	−14.36	−11.38	298.37
		Rice	-	-	1.62	-	-	-	-	−43.99	−22.66	11.02
		Nakagami	-	-	-	1.41	-	-	-	−22.95	−26.68	−91.79
		α-μ	1.85	-	-	1.51	-	-	-	−22.71	−27.73	−116.55
		κ-μ	-	-	0.66	1.28	-	-	-	−35.27	−33.59	−266.31
		κ-1/2 (FN)	-	-	4.39	-	-	-	-	−50.43	−21.30	47.83
		κ-3/2	-	-	≈ 0	-	-	-	-	−24.25	−24.24	−29.46
		η-μ	-	0.96	-	0.74	-	-	-	−26.36	−22.59	14.70
		α-η-κ-μ	1.74	1.19	3.49	1.69	3.78	≈ 0	3.41	−154.03	**−47.15**	**−603.02**

Moreover, in general, the propagation environment is very complex, and no single or simple modeling can comprise all the existing phenomena.

VI. CONCLUSION

Short-term fading characterization in the recently standardized 5G mm-wave band has been very scarcely explored, if not unexplored at all. To fill this gap, this paper further the knowledge of the short-term fading channel in the mentioned bands. To that end, a thorough measurement campaign has been conducted in an indoor environment in the mm-wave range at frequencies 26, 28 and 39 GHz, as standardized by the ITU for 5G systems. Measurements have been performed in a variety of scenarios, under LoS and nLoS conditions.

First and second order statistics of representative fading models, namely Rayleigh, Rice, Nakagami, folded Normal, α-μ, η-μ, κ-μ, and α-η-κ-μ have been investigated. From the experimental data, the parameters of the mentioned distributions have been estimated using the Matlab least-square-error based function and the corresponding curves of the theoretical models have been compared with the empirical ones and the best model have been selected using three different figures of merit, namely NMSE, KS, and AIC. From the results of the first order statistical tests, considering the NMSE and the KS criteria, the more general distributions have performed better than the simpler ones, as expected, because they are more flexible. When considering the AIC metric, we find that in some cases, though few, the conventional distributions obtained the best compromise solution, since, as known, AIC penalizes the distributions with greater number of parameters. However, in the great majority of the situations, the more general distributions still provided the best adjustment, indeed justifying their use. As far as the second-order statistical tests are concerned, in all evaluated scenarios and for the three considered frequencies, the best performance has been achieved by the α-η-κ-μ distribution. Followed by it, the other less but still general models, namely α-μ, η-μ, κ-μ, offer the best results. It is also observed that in some situations, the lower tail of the true empirical LCR, which is the lower signal-to-noise region, obtained with field data, can only be followed by the more general fading model, because of its inherent flexibility and nonunimodality.

In addition, the theory concerning the κ-μ model has been further advanced with the derivation of new, simpler expressions concerning its first and second order statistics for the special cases in which $\mu = n + 1/2$ in which $n \in \mathbb{N}$.

Through what has been observed in our investigation, it can be concluded that the well-known fading models available in the literature can be satisfactorily used to characterize both first- and second-order short-term fading statistics of the standardized 5G mm-wave bands in an indoor environment where there are many reflecting and dispersing elements. As a matter of pure speculation, we conjecture that these results could be extended for other environments. However, this still remains as a subject of investigation. The best fitting performances, however, are obtained by the more general fading models, with a performance-versus-complexity compromise best attained by α-μ, η-μ, κ-μ. Of course, a more refined adjustment is always achieved by α-η-κ-μ but at a high complexity cost.

REFERENCES

[1] International Telecommunication Union, "Final acts (WRC-19)," in *Proc. World Radiocommunication Conf.*, Sharm el-Sheikh, Egypt, Oct./Nov. 2019.

[2] M. R. Akdeniz, Y. Liu, M. K. Samimi, S. Sun, S. Rangan, T. S. Rappaport, and E. Erkip, "Millimeter wave channel modeling and cellular capacity evaluation," *IEEE J. Sel. Areas Commun.*, vol. 32, no. 6, pp. 1164–1179, Jun. 2014.

[3] M.-W. Jung, J. Kim, and Y.-K. Yoon, "Measurements of path loss in MM-wave for indoor environments," in *Proc. Asia Pacific Microw. Conf.*, Dec. 2009, pp. 1068–1071.

[4] D. M. Matic, H. Harada, and R. Prasad, "Indoor and outdoor frequency measurements for MM-waves in the range of 60 GHz," in *Proc. 48th IEEE Veh. Technol. Conf. Pathway Global Wireless Revolution (VTC)*, vol. 1, May 1998, pp. 567–571.

[5] X. Zhang, G. Qiu, J. Zhang, L. Tian, P. Tang, and T. Jiang, "Analysis of millimeter-wave channel characteristics based on channel measurements in indoor environments at 39 GHz," in *Proc. 11th Int. Conf. Wireless Commun. Signal Process. (WCSP)*, Oct. 2019, pp. 1–6.

[6] Q. Liao, Z. Ying, and C. Gustafson, "Simulations and measurements of 15 and 28 GHz indoor channels with different array configurations," in *Proc. Int. Workshop Antenna Technol., Small Antennas, Innov. Struct., Appl. (iWAT)*, 2017, pp. 256–259.

[7] T. Zwick, T. J. Beukema, and H. Nam, "Wideband channel sounder with measurements and model for the 60 GHz indoor radio channel," *IEEE Trans. Veh. Technol.*, vol. 54, no. 4, pp. 1266–1277, Jul. 2005.

[8] H. Xu, V. Kukshya, and T. S. Rappaport, "Spatial and temporal characteristics of 60-GHz indoor channels," *IEEE J. Sel. Areas Commun.*, vol. 20, no. 3, pp. 620–630, Apr. 2002.

[9] C. R. Anderson and T. S. Rappaport, "In-building wideband partition loss measurements at 2.5 and 60 GHz," *IEEE Trans. Wireless Commun.*, vol. 3, no. 3, pp. 922–928, May 2004.

[10] P. Smulders, "Statistical characterization of 60-GHz indoor radio channels," *IEEE Trans. Antennas Propag.*, vol. 57, no. 10, pp. 2820–2829, Oct. 2009.

[11] H. J. Thomas, R. S. Cole, and G. L. Siqueira, "An experimental study of the propagation of 55 GHz millimeter waves in an urban mobile radio environment," *IEEE Trans. Veh. Technol.*, vol. 43, no. 1, pp. 140–146, Feb. 1994.

[12] M. Kyro, K. Haneda, J. Simola, K.-I. Takizawa, H. Hagiwara, and P. Vainikainen, "Statistical channel models for 60 GHz radio propagation in hospital environments," *IEEE Trans. Antennas Propag.*, vol. 60, no. 3, pp. 1569–1577, Mar. 2012.

[13] T. S. Rappaport, S. Sun, R. Mayzus, H. Zhao, Y. Azar, K. Wang, G. N. Wong, J. K. Schulz, M. Samimi, and F. Gutierrez, "Millimeter wave mobile communications for 5G cellular: It will work!" *IEEE Access*, vol. 1, pp. 335–349, 2013.

[14] S. Hur, S. Baek, B. Kim, Y. Chang, A. F. Molisch, T. S. Rappaport, K. Haneda, and J. Park, "Proposal on millimeter-wave channel modeling for 5G cellular system," *IEEE J. Sel. Topics Signal Process.*, vol. 10, no. 3, pp. 454–469, Apr. 2016.

[15] K. Haneda, J. Jarvelainen, A. Karttunen, M. Kyro, and J. Putkonen, "Indoor short-range radio propagation measurements at 60 and 70 GHz," in *Proc. 8th Eur. Conf. Antennas Propag. (EuCAP)*, Apr. 2014, pp. 634–638.

[16] M.-S. Choi, G. Grosskopf, and D. Rohde, "Statistical characteristics of 60 GHz wideband indoor propagation channel," in *Proc. IEEE 16th Int. Symp. Pers., Indoor Mobile Radio Commun.*, vol. 1, Sep. 2005, pp. 599–603.

[17] M. K. Samimi, G. R. MacCartney, S. Sun, and T. S. Rappaport, "28 GHz millimeter-wave ultrawideband small-scale fading models in wireless channels," in *Proc. IEEE 83rd Veh. Technol. Conf. (VTC Spring)*, May 2016, pp. 1–6.

[18] T. Mavridis, L. Petrillo, J. Sarrazin, A. Benlarbi-Delai, and P. De Doncker, "Near-body shadowing analysis at 60 GHz," *IEEE Trans. Antennas Propag.*, vol. 63, no. 10, pp. 4505–4511, Oct. 2015.

[19] J. Reig, M.-T. Martinez-Inglés, L. Rubio, V.-M. Rodrigo-Penarrocha, and J.-M. Molina-García-Pardo, "Fading evaluation in the 60 GHz band in line-of-sight conditions," *Int. J. Antennas Propag.*, vol. 2014, p. 12, Aug. 2014.
[20] J. Reig, V. M. R. Peñarrocha, L. Rubio, M. T. Martínez-Inglés, and J. M. Molina-García-Pardo, "The folded normal distribution: A new model for the small-scale fading in line-of-sight (LOS) condition," *IEEE Access*, vol. 7, pp. 77328–77339, 2019.
[21] T. R. R. Marins, A. A. dos Anjos, V. M. R. Penarrocha, L. Rubio, J. Reig, R. A. A. de Souza, and M. D. Yacoub, "Fading evaluation in the mm-wave band," *IEEE Trans. Commun.*, vol. 67, no. 12, pp. 8725–8738, Dec. 2019.
[22] A. A. Dos Anjos, T. R. R. Marins, C. R. N. Da Silva, V. M. R. Penarrocha, L. Rubio, J. Reig, R. A. A. De Souza, and M. D. Yacoub, "Higher order statistics in a mmWave propagation environment," *IEEE Access*, vol. 7, pp. 103876–103892, 2019.
[23] J. E. Gentle, *Random Number Generation and Monte Carlo Methods*, 2nd ed. New York, NY, USA: Springer-Verlag, 2004.
[24] Wolfram Res., Champaign, IL, USA. (2016). *Wolfram Functions*. Accessed: Jan. 2, 2020. [Online]. Available: http://functions.wolfram.com/id
[25] A. Prudnikov, *Integrals and Series: Elementary Functions*, vol. 1. New York, NY, USA: Gordon & Breach Science, 1986.
[26] M. Abramowitz, *Handbook of Mathematical Functions, With Formulas, Graphs, and Mathematical Tables*. New York, NY, USA: Dover, 1974.
[27] C. Sanchis Borrás, J. Molina-García-Pardo, L. Rubio, J. Pascual-García, V. M. Rodrigo Pe narrocha, L. Juan Llàcer, and J. Reig, "Millimeter wave MISO-OFDM transmissions in an intra-wagon environment," *IEEE Trans. Intell. Transp. Syst.*, early access, Apr. 7, 2020, doi: 10.1109/TITS.2020.2983028.
[28] L. Rubio, R. P. Torres, V. M. Rodrigo Peñarrocha, J. R. Pérez, H. Fernández, J.-M. Molina-Garcia-Pardo, and J. Reig, "Contribution to the channel path loss and time-dispersion characterization in an office environment at 26 GHz," *Electronics*, vol. 8, no. 11, p. 1261, Nov. 2019.
[29] *MathWorks*. Accessed: Nov. 16, 2020. [Online]. Available: https://www.mathworks.com/help/optim/ug/lsqcurvefit.html

TIAGO REIS RUFINO MARINS received the B.S.E.E. and M.Sc. degrees from the National Institute of Telecommunication (INATEL), Brazil, in 2008 and 2012, respectively, and the Ph.D. degree from the State University of Campinas (UNICAMP), Campinas, Brazil, in 2021. He is currently working as a Researcher with the Radiocommunication Reference Center (RRC), INATEL. His research interests include channel coding, wireless communications, and channel modeling.

ANDRÉ ANTÔNIO DOS ANJOS received the B.S.E.E. and M.Sc. degrees from the National Institute of Telecommunication (INATEL), Brazil, in 2009 and 2012, respectively, and the Ph.D. degree from the State University of Campinas (UNICAMP), Campinas, Brazil, in 2021. He currently works as an Engineer with the Inatel Competence Center (ICC). His research interests include wireless communications, fading channel modeling, non-linear systems, and spectrum sensing.

CARLOS RAFAEL NOGUEIRA DA SILVA is currently a Professor with the Electrical and Engineering Department, Federal University of Triangulo Mineiro. His research interests include wireless channel modeling, spectrum sensing, cognitive radio, composite channel characterization and applications, and wireless communications in general.

VICENT MIQUEL RODRIGO PEÑARROCHA received the Ph.D. degree in telecommunications engineering from the Universitat Politécnica de València (UPV), Spain, in 2003. He joined as a Lecturer with the Departamento de Comunicaciones, UPV, in 1991. His current research interests include radiowave propagation, antenna measurements, and instrumentation.

LORENZO RUBIO (Senior Member, IEEE) received the Ph.D. degree in telecommunications engineering from the Universitat Politécnica de València (UPV), Spain, in 2004. In 1996, he joined the Communications Department, UPV, where he is currently a Full Professor of telecommunications engineering. His research interests include radiowave propagation, ultra-wideband (UWB) systems, vehicular communications, and millimetre wave (mmWave) propagation.

JUAN REIG (Senior Member, IEEE) received the Ph.D. degree in telecommunications engineering from the Universitat Politécnica de València (UPV), Spain, in 2000. Since 1994, he has been a Faculty Member with the Department of Communications, UPV, where he is currently a Full Professor of telecommunication engineering. His research interests include fading theory, diversity, ultra-wideband (UWB) systems, vehicular communications, and millimeter wave (mmWave) propagation.

RAUSLEY ADRIANO AMARAL DE SOUZA (Senior Member, IEEE) received the B.S.E.E. and M.Sc. degrees from the National Institute of Telecommunication (INATEL), Brazil, in 1994 and 2002, respectively, and the Ph.D. degree from the State University of Campinas (UNICAMP), Campinas, Brazil. Prior to joining the Academy, he worked in industry. He joined the INATEL, in 2002, where he is a Full Professor. His research interest includes wireless communications.

MICHEL DAOUD YACOUB (Member, IEEE) received the Ph.D. degree from the University of Essex, England, in 1988. He joined the School of Electrical and Computer Engineering, UNICAMP, Brazil, in 1989, where he is a Full Professor. Prior to joining the Academy, he worked in industries. His research interest includes wireless communications.